Laser-plasma interactions in magnetized environment

Yuan Shi, Hong Qin, and Nathaniel J. Fisch

Citation: Physics of Plasmas **25**, 055706 (2018); doi: 10.1063/1.5017980
View online: https://doi.org/10.1063/1.5017980
View Table of Contents: http://aip.scitation.org/toc/php/25/5
Published by the American Institute of Physics

Laser-plasma interactions in magnetized environment

Yuan Shi,[1,2,a),b)] Hong Qin,[1,2,3] and Nathaniel J. Fisch[1,2]
[1]*Department of Astrophysical Sciences, Princeton University, Princeton, New Jersey 08544, USA*
[2]*Princeton Plasma Physics Laboratory, Princeton University, Princeton, New Jersey 08543, USA*
[3]*School of Nuclear Science and Technology and Department of Modern Physics, University of Science and Technology of China, Hefei, Anhui 230026, China*

(Received 1 December 2017; accepted 17 January 2018; published online 14 March 2018)

Propagation and scattering of lasers present new phenomena and applications when the plasma medium becomes strongly magnetized. With mega-Gauss magnetic fields, scattering of optical lasers already becomes manifestly anisotropic. Special angles exist where coherent laser scattering is either enhanced or suppressed, as we demonstrate using a cold-fluid model. Consequently, by aiming laser beams at special angles, one may be able to optimize laser-plasma coupling in magnetized implosion experiments. In addition, magnetized scattering can be exploited to improve the performance of plasma-based laser pulse amplifiers. Using the magnetic field as an extra control variable, it is possible to produce optical pulses of higher intensity, as well as compress UV and soft x-ray pulses beyond the reach of other methods. In even stronger giga-Gauss magnetic fields, laser-plasma interaction enters a relativistic-quantum regime. Using quantum electrodynamics, we compute a modified wave dispersion relation, which enables correct interpretation of Faraday rotation measurements of strong magnetic fields. *Published by AIP Publishing.*
https://doi.org/10.1063/1.5017980

I. INTRODUCTION

Magnetic fields affect laser propagation and scattering when the electron gyrofrequency $\Omega_e = eB/m_e$ is no longer ignorable when compared to the laser frequency. For example, a magnetic field $\sim$10 MG, corresponding to $\Omega_e\hbar \sim 0.1$ eV, will noticeably alter the wave dispersion relation and the scattering cross section of optical lasers in plasmas. In low density plasmas, the role of the strong magnetic field is largely classical. However, as plasma density increases, quantum effects may emerge when the characteristic size of electron wave function $l_B = \sqrt{2\hbar/eB}$ becomes comparable to inter-particle spacing. For example, a magnetic field $\sim$10 MG, corresponding to the magnetic de Broglie wavelength $l_B \sim 1$ nm, may already allow electrons to feel the Fermi degeneracy in solid-density plasmas. As the field strength further increases towards the Schwinger limit $B_c \sim 10^{13}$ G, where the magnetic de Broglie wavelength shrinks to electron Compton wavelength, relativistic-quantum effects of magnetic fields will become increasingly prominent.

While magnetic fields on the order of Schwinger limit can only be found near neutron stars, mega-Gauss to giga-Gauss magnetic fields can already be produced by a number of laboratory techniques. For example, using lasers to drive plasma implosions, seed magnetic fields, either self-generated[1] or externally imposed,[2,3] can be amplified to tens of mega-Gauss by magnetic flux compression. A more controllable technique produces magnetic fields of similar strengths using lasers to drive capacitor-coil targets.[4–6] Comparable or even stronger magnetic fields can be produced by dynamo effects when solid targets are directly ablated by intense laser pulses.[7–13] Using these techniques, magnetic fields may be further intensified by employing stronger drive lasers. This emerging availability of very strong magnetic fields thus presents new challenges and opportunities that remain to be investigated. In this paper, we review three research directions where effects of strong magnetic fields during laser-plasma interactions have been explored.

The first direction is coherent scattering of lasers, for which magnetic fields on the order of mega-Gauss can make noticeable differences for 1-μm lasers. Coherent scattering happens when the Debye length of the plasma is not much larger than the laser wavelength. In this case, instead of interacting directly with individual charged particles,[14] lasers interact collectively with plasma waves and scatter due to nonlinear motion of the plasma medium. Magnetized waves that scatter lasers are Alfvén waves, hybrid waves, and Bernstein waves,[15] which replace the Langmuir wave and the ion-acoustic wave in unmagnetized plasmas. Consequently, Raman and Brillouin scattering,[16] the two coherent scattering modes in unmagnetized plasmas, are now replaced by scattering mediated by magnetized plasma waves, on which the magnetic anisotropy is imprinted.[17] Understanding angular dependence due to the anisotropy is especially important for magnetized laser implosion experiments,[18,19] where multiple laser beams propagate at angles with respect to the magnetic field.

The second direction is laser pulse compression mediated by magnetized plasmas, for which tens of mega-Gauss magnetic fields bring significant improvements when amplifying 1-μm lasers. During laser pulse compression,[20] energy stored in a long pump laser is transferred, via a plasma wave, to a seed pulse, whose intensity is amplified and the duration is shortened. While laser pulses beyond the reach of Chirped Pulse Amplification (CPA)[26] may already be produced using

Note: Paper CI3 4, Bull. Am. Phys. Soc. **62**, 64 (2017).
[a)]Invited speaker.
[b)]Electronic mail: yshi@pppl.gov

Raman[21,22] or Brillouin[23–25] compression in unmagnetized plasmas, magnetic fields bring additional improvements.[27] For optical lasers, the improvements are largely engineering, where external magnetic fields allow better control of plasma uniformity. On the other hand, for shorter wavelength lasers, the improvements due to alleviation of physical constraints, such as damping and instabilities, become more substantial. Due to these improvements, magnetized mediations may be used to compress intense UV and soft x-ray pulses, which cannot be compressed using other methods.

The third direction is laser propagation, which remains largely classical until magnetic fields on the order of giga-Gauss are present. Although giga-Gauss magnetic fields are still far below the Schwinger limit, relativistic-quantum effects may already become observable when they are boosted near singularities. For example, relativistic-quantum effects can noticeably alter the dependency of Faraday rotation on the frequency of lasers, especially when the frequency approaches the cutoff frequency of the right-circularly polarized (R) wave. When approaching the R-wave cutoff, the phase velocity of the R wave goes to infinity, while the phase velocity of the left-circularly polarized (L) wave remains finite. Therefore, the difference in phase velocities, which leads to Faraday rotation of linearly polarized lasers, becomes singular. This singularity boosts relativistic-quantum effects and can produce order unity corrections to Faraday rotation in strongly magnetized plasmas.[28] Not surprisingly, when the magnetic field becomes even stronger, relativistic-quantum effects will become more appreciable.

This paper reviews progress made in these three research directions and motivates future endeavors towards understanding and utilizing magnetic fields during laser-plasma interactions. In Sec. II, we present coherent laser scattering in magnetized plasmas, using results from a cold-fluid theory as an illustration. In Sec. III, we demonstrate an application of strong magnetic fields, using laser pulse compression as an example. In Sec. IV, we discuss the new regime that strong magnetic fields enable us to reach, by studying how relativistic-quantum effects modify Faraday rotation as an example. In Sec. V, we summarize challenges and opportunities, as strong magnetic fields become available.

II. COHERENT THREE-WAVE SCATTERING

Coherent scattering is a primary way by which long wavelength lasers are scattered in high-density plasmas. To put this type of scattering in the context of other scattering mechanisms, notice that the degree of coherence of laser scattering can vary, depending on the wavelength of the laser. Incoherent scattering is the extreme where the wavelength of the laser is much smaller than the particle correlation length. In this case, the laser resolves the discreteness of the medium and directly wiggles individual particles, which radiate secondary electromagnetic (EM) waves as scattered lights. In the other extreme, coherent scattering happens when the wavelength of the laser is much larger than the particle correlation length. In this case, motion of charged particles is highly synchronized, and the laser scatters due to collective nonlinear response of the plasma medium. In this section, we will focus on coherent scattering of an incident laser due to resonant three-wave interactions.

A. Resonant three-wave interactions

The lowest order nonlinearities couple three waves, and resonant three-wave interactions can happen when frequencies ω_i and wave vectors $\mathbf{k}_i$ of the three waves satisfy the resonance conditions

$$\omega_1 = \omega_2 + \omega_3, \tag{1}$$

$$\mathbf{k}_1 = \mathbf{k}_2 + \mathbf{k}_3, \tag{2}$$

where all ω_i values are positive. These resonance conditions only need to be satisfied approximately, because large amplitude waves can have a finite band width. Moreover, when two of these three waves are strongly driven by external sources, the third wave does not need to be a linear eigenmode of the system.

When all three waves are eigenmodes of the homogeneous system, their envelopes evolve slowly due to their weak resonant coupling. The evolution of wave envelopes can be described by the three-wave equations[29]

$$d_t a_1 = -\frac{\Gamma}{\omega_1} a_2 a_3, \tag{3}$$

$$d_t a_2 = \frac{\Gamma}{\omega_2} a_3 a_1, \tag{4}$$

$$d_t a_3 = \frac{\Gamma}{\omega_3} a_1 a_2, \tag{5}$$

where $d_t a_i := (\partial_t + \mathbf{v}_{gi} \cdot \nabla + \nu_i) a_i$ denotes the advective derivative. In the above equations, the real-valued $a_i = eE_i u_i^{1/2}/m_e c\omega_i$ is the normalized wave electric field, where u_i is the coefficient such that the averaged energy of the linear wave is $U_i = \epsilon_0 u_i E_i^2/2$. The normalized wave amplitude a_i is advected at the wave group velocity $\mathbf{v}_{gi} = \partial\omega_i/\partial\mathbf{k}_i$, and is damped at a rate ν_i. As the waves advect, they transfer energy between each other at a rate determined by Γ, the coupling coefficient.

B. Coupling coefficient

While resonant three-wave interactions can always be described by the same three-wave equations, the coupling coefficient is what encodes the physical details. This essential coefficient was very difficult to compute in the presence of a background magnetic field. Although many methods were attempted,[30–37] explicit expressions of the coupling coefficient were only known in the simple cases where the collimated waves propagate either parallel[38] or perpendicular[39–41] to the magnetic field. Recently, we have obtained a convenient formula for the coupling coefficient in cold magnetized plasmas when waves propagate at arbitrary angles[17]

$$\Gamma = \sum_s \frac{\zeta_s \omega_{ps}^2 \mathrm{Re}(\Theta^s)}{4(u_1 u_2 u_3)^{1/2}}. \tag{6}$$

In the above formula, ω_{ps} is the plasma frequency of species s, whose charge-to-mass ratio $\zeta_s = e_s m_e/e m_s$ is normalized by the ratio of electrons.

The most important term in the coupling coefficient is the real part of the normalized scattering strength

$$\Theta^s = \Theta^s_{1,\bar{2}\bar{3}} + \Theta^s_{\bar{2},\bar{3}1} + \Theta^s_{\bar{3},1\bar{2}} + \Theta^s_{1,\bar{3}\bar{2}} + \Theta^s_{\bar{2},1\bar{3}} + \Theta^s_{\bar{3},\bar{2}1}. \tag{7}$$

This linear superposition of the strengths of six scattering channels corresponds to $3! = 6$ ways the three waves can couple through the interaction Lagrangian. In Eq. (7), we use notations $\omega_{\bar{j}} = -\omega_j$, $\mathbf{k}_{\bar{j}} = -\mathbf{k}_j$, and $\mathbf{e}_{\bar{j}} = \mathbf{e}_j^*$. Using these notations, the normalized strength of each scattering channel is given by the simple expression

$$\Theta^s_{i,jl} = \frac{1}{\omega_j}(c\mathbf{k}_i \cdot \mathbb{F}^s_j \mathbf{e}_j)(\mathbf{e}_i \cdot \mathbb{F}^s_l \mathbf{e}_l), \tag{8}$$

where $\mathbf{e}_j$ is the complex unit polarization vector of the jth wave. Notice that the relative phases between the three waves are important. The maximum coupling is attained when $|\mathrm{Re}(C)| = |C|$, where $C = \sum_s \zeta_s \omega^2_{ps} \Theta^s$. This happens when the phases of $\mathbf{e}_j$'s are synchronized.

The forcing operator $\mathbb{F}^s_j$, which appears in the scattering strengths, is related to the linear susceptibility χ^s_j by $\chi^s_j = -\omega^2_{ps}\mathbb{F}^s_j/\omega^2_j$. For example, in a cold-fluid plasma where gyro radii are much smaller than the wavelength, the forcing operator is such that

$$\mathbb{F}^s_j \mathbf{z} = \gamma^2_{s,j}\Big[\mathbf{z} + i\beta_{s,j}\mathbf{z}\times\mathbf{b} - \beta^2_{s,j}(\mathbf{z}\cdot\mathbf{b})\mathbf{b}\Big], \tag{9}$$

for any complex vector $\mathbf{z} \in \mathbb{C}^3$. Here, $\mathbf{b}$ is the unit vector along the background magnetic field, $\gamma^2_{s,j} = 1/(1-\beta^2_{s,j})$ is the magnetization factor, and $\beta_{s,j} = \Omega_s/\omega_j$ is the magnetization ratio. Based on the universality of the interaction Lagrangian, we speculate that thermal effects might be incorporated by replacing the above cold-fluid forcing operator with one that corresponds to the warm plasma susceptibility.

Finally, the last set of terms in the coupling coefficient is the wave energy coefficients

$$u_j = \frac{1}{2}\mathbf{e}_j^\dagger \mathbb{H}_j \mathbf{e}_j. \tag{10}$$

Here, $\mathbb{H}_j = \partial(\omega_j^2\epsilon_j)/\omega_j\partial\omega_j$ is the wave energy operator, where $\epsilon_j = 1 + \sum_s \chi^s_j$ is the dielectric tensor. In terms of the forcing operator, the wave energy operator can be written as

$$\mathbb{H}_j = 2\mathbb{I} - \sum_s \frac{\omega^2_{ps}}{\omega_j}\frac{\partial \mathbb{F}^s_j}{\partial\omega_j}. \tag{11}$$

Using the above formulas, the coupling coefficient between any three resonant eigenmodes can be readily evaluated in the most general geometry.

C. Experimental observables

To illustrate how the coupling coefficient can be related to experimental observables, let us consider Stokes scattering. As the incident electromagnetic (*EM*) wave a_1 propagates, it may pump the growth of some fluctuations a_3 in the plasma, while being scattered into a_2 as some frequency down-shifted *EM* wave. In the linear stage, the pump amplitude is roughly constant, and the Stokes scattering results in parametric growth of the scattered *EM* wave at an exponential rate

$$\gamma_0 = \frac{|\Gamma a_1|}{\sqrt{\omega_2\omega_3}}, \tag{12}$$

when damping and spatial variations are ignorable. To get a sense of how large this growth rate is, we can compare it with Raman scattering $\gamma_0 = \gamma_R\mathcal{M}$, where the normalized growth rate

$$\mathcal{M} = 2\frac{|\Gamma|}{\omega_p^2}\left(\frac{\omega_p^3}{\omega_1\omega_2\omega_3}\right)^{1/2}, \tag{13}$$

and $\gamma_R = \sqrt{\omega_1\omega_p}|a_1|/2$ the backward Raman growth rate in an unmagnetized plasma of the same density. Here, $\omega_p^2 = \sum_s \omega^2_{ps}$ is the total plasma frequency. In experiments, most signals will come from the largest growth rate, for which wave phases are auto-synchronized.

To evaluate the growth rate, we can imagine what happens in experiments, in which the frequency ω_1 of the incident laser and its direction of propagation $\hat{\mathbf{k}}_1$ are controlled. Given these control variables and plasma parameters, the pump laser can be a superposition of the two *EM* eigenmodes. The eigenmode k_1^- with longer wavelength is the *R* wave when $\hat{\mathbf{k}}_1 \parallel \mathbf{B}_0$, and it smoothly deforms to the extraordinary (*X*) wave when $\hat{\mathbf{k}}_1 \perp \mathbf{B}_0$. On the other hand, the eigenmode k_1^+ with shorter wavelength smoothly deforms from the *L* wave to the ordinary (*O*) wave when θ_1, the angle between $\hat{\mathbf{k}}_1$ and $\mathbf{B}_0$, increases from 0° to 90°. Suppose the experiment setup selects one of the eigenmodes, then the wave vector $\mathbf{k}_1$ and the wave polarization $\mathbf{e}_1$ are fixed. We can then make observations in the $\hat{\mathbf{k}}_2$ direction, which has polar angle θ_2 measured from $\mathbf{B}_0$ and azimuthal angle ϕ_2 measured from the $\mathbf{k}_1\mathbf{B}_0$ plane. The frequency ω_2 of the scattered light can be measured using some spectrometer, and the polarization $\mathbf{e}_2$ can be selected using some waveplates and filters. If $\omega_3 = \omega_1 - \omega_2$ and $\mathbf{k}_3 = \mathbf{k}_1 - \mathbf{k}_2$ correspond to an eigenmode of the plasma, then resonant three-wave scattering can happen, and the spectrometer will display a peak centered at ω_2, whose height is related to the normalized growth rate.

As an example, we evaluate the normalized growth rate of a 1.06-μm Nd:glass laser in a magnetized hydrogen plasma, when the incident laser propagates at polar angle $\theta_1 = 30°$ in the k_1^+ eigenmode (Fig. 1). We take the density of the fully ionized plasma to be $n_0 = 10^{19}\mathrm{cm}^{-3}$, which is typical for gas jet plasmas. In addition, we take the magnetic field $B_0 = 8.12$ MG, achievable using current technology. In this plasma, the laser frequency $\omega_1 \approx 10\omega_p$, $|\Omega_e| \approx 0.8\omega_p$, and the magnetic field plays an important role in coherent Stokes scattering. In two-species cold plasmas, there exist three branches of magnetized plasma waves, each resulting in a different angular dependence of the normalized growth rate. First, in this over-dense plasma ($\omega_p > |\Omega_e|$), the upper

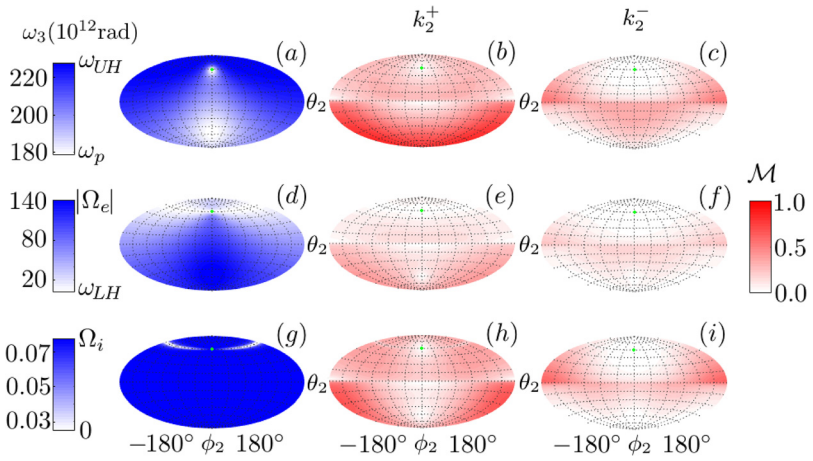

FIG. 1. Coherent scattering of an incident laser in the k_1^+ eigenmode, propagating ($\theta_1 = 30°, \phi_1 = 0°$, green dots) in a magnetized cold hydrogen plasma with $\omega_p \approx \omega_1/10$ and $|\Omega_e| \approx 0.8\omega_p$. For scattering off the u-branch waves (upper panel), the frequency down shift (a) is between ω_p and ω_{UH}. The normalized growth rate $\mathcal{M}^+$ of the k_2^+ eigenmode (b) is suppressed in polarization-forbidden regions near the equatorial plane ($\theta_2 \approx 90°$), while the normalized growth rate $\mathcal{M}^-$ of the k_2^- eigenmode (c) is polarization-forbidden in forward ($\theta_2 = \theta_1, \phi_2 = 0°$) and backward ($\theta_2 = 180° - \theta_1, \phi_2 = \pm 180°$) directions. For scattering off the l-branch waves (middle panel), the frequency down shift (d) is between ω_{LH} and $|\Omega_e|$. In addition to polarization forbidden regions, the growth rate $\mathcal{M}^+$ (e) and $\mathcal{M}^-$ (f) are suppressed in interference-forbidden regions where electron and ion scatterings cancel (near $\theta_2 \approx \theta_1$), as well as in energy-forbidden regions where $\omega_3 \approx |\Omega_e|$. Finally, the incident laser can scatter off the b-branch waves (bottom panel). The frequency down shift (g) is between zero and Ω_i, and the growth rates $\mathcal{M}^+$ (h) and $\mathcal{M}^-$ (i) are suppressed in polarization-forbidden regions, as well as in energy-forbidden regions.

(u) branch is the Langmuir wave when $\mathbf{k}_3 \parallel \mathbf{B}_0$. The u branch becomes the upper-hybrid (UH) wave when $\mathbf{k}_3 \perp \mathbf{B}_0$, whose frequency $\omega_{UH} \simeq \sqrt{\omega_p^2 + \Omega_e^2}$ in the large-k_3 limit. For scattering off the u branch, the frequency down shift [Fig. 1(a)] is between ω_p and ω_{UH}. For the k_2^+ eigenmode, backscattering is favored while scattering perpendicular to $\hat{\mathbf{k}}_1$, where $\mathbf{e}_1^\dagger \mathbf{e}_2 \approx 0$, is forbidden [Fig. 1(b)]. On the contrary, the polarization of the k_2^- eigenmode is such that forward and backward scattering are forbidden, while perpendicular scattering is allowed [Fig. 1(c)]. Second, the EM waves can scatter from the lower (l) branch plasma wave. The l branch is the electron-cyclotron wave when $\mathbf{k}_3 \parallel \mathbf{B}_0$, and it becomes the lower-hybrid (LH) wave when $\mathbf{k}_3 \perp \mathbf{B}_0$, whose frequency $\omega_{LH} \simeq \sqrt{|\Omega_e|\Omega_i \omega_p/\omega_{UH}}$ in the large-k_3 limit. For scattering from the l branch, the frequency down shift [Fig. 1(d)] is between ω_{LH} and $|\Omega_e|$. In addition to polarization-forbidden regions, both the k_2^+ [Fig. 1(e)] and the k_2^- [Fig. 1(f)] scatterings encounter special angles where electron and ion scattering destructively interfere and therefore cancel one another (near $\theta_2 \approx \theta_1$). Finally, the bottom ($b$) branch is the Alfvén wave in the small-k_3 limit, and becomes the ion-cyclotron wave in the large-k_3 limit. For scattering off the bottom (b) branch, the frequency down shift [Fig. 1(g)] is between zero and Ω_i. Both the k_2^+ [Fig. 1(h)] and the k_2^- [Fig. 1(i)] scatterings encounter energy forbidden regions near $\theta_2 \approx \theta_1$, where plasma waves are energetically too expensive to excite. Away from these polarization-, interference-, and energy-forbidden regions where $u_i \gg |\Theta^s|$, coherent Stokes scattering from magnetized plasma waves has growth rates comparable to that of Raman backscattering.

III. LASER PULSE COMPRESSION

While coherent scattering may be unwanted in laser implosion experiments, it can, on the other hand, be utilized to amplify laser pulses beyond what is achievable using other techniques. The current state-of-the-art technique is Chirped Pulse Amplification[26] (CPA), which can produce optical pulses with unfocused intensity $\sim 10^{14}\text{W/cm}^2$, beyond which the solid grating, an essential component of CPA, is likely to be damaged.[42,43] Although laser intensity may be further increased by focusing, the CPA technique is not applicable to shorter wavelength lasers, such as excimer UV lasers[44] and free-electron x-ray lasers.[45,46] However, such high-intensity short-wavelength lasers are required in many applications, including inertial confinement fusion[47,48] and single molecule imaging.[49,50] Hence, techniques that can amplify and shorten these pulses are highly demanded. A promising technique is plasma-based laser pulse compression. This technique contemplated using unmagnetized plasma as the gain medium, which only supports the Langmuir mode[21] and the Brillouin mode[51] as mediating waves. By magnetizing the plasma medium, more waves become available. We can thus increase the intensity of optical pulses, as well as extend pulse compression to the soft x-ray regime,[27] which was not accessible using previous methods. In this section, we use UH-wave mediation as an example to demonstrate benefits of applying external magnetic fields in laser pulse compression.

A. Mediation by the upper-hybrid wave

In magnetized plasmas, one of the many waves that can be utilized to mediate laser pulse compression is the UH wave. The UH wave is the asymptote of one branch of the electron Bernstein waves in the low temperature limit. Since $\omega_{UH} \simeq \sqrt{\omega_p^2 + \Omega_e^2}$, the external magnetic field partially replaces the role of plasma density in the three-wave resonance conditions. In other words, by applying a magnetic field transverse to the direction of laser propagation, the plasma density required to match the resonance conditions can be reduced.

The reduction of requisite plasma density has immediate engineering benefits. First, challenging technology for producing high-density plasmas can now be substituted by available technologies for generating strong magnetic fields. The plasma density required to compress 1-μm pulses using unmagnetized plasmas is $\sim 10^{19}\mathrm{cm}^{-3}$, which is already at the verge of what is feasible with gas jet plasmas. To compress shorter wavelength lasers using unmagnetized plasmas, denser plasma targets, such as foams and aerosol jets,[52] remain to be developed. Allowing dense plasmas to be replaced by magnetic fields thus relaxes the engineering challenges. Second, uniformity of the plasma target becomes more controllable when magnetic fields supply the resonance frequency. While it is difficult to control the internal plasma density, adding an external magnetic field introduces an extra control variable, which may be adjusted to maintain the three-wave resonance conditions, and tune the performance of laser pulse compressors.

When the *UH* wave mediates resonant energy transfer between a given pump laser and a given seed pulse, the lower plasma density results in a slower linear growth rate[27] $\gamma_0 = \sqrt{\omega_3\omega_1}|a_1|/2\gamma_3$, where $\gamma_3 = \omega_3/\omega_p > 1$ is the electron magnetization factor, defined in Sec. II. Other than a smaller growth rate, laser pulse compression mediated by the *UH* wave is similar to Raman compression.[21] After the linear stage of the amplification, the pump amplitude a_1 starts to deplete. At this pump depletion stage, the steep front of the seed pulse keeps on growing, whereas the tail of the pulse starts to decay. This asymmetric growth of the seed pulse results in an effective compression of the laser pulse. After the seed pulse transits the entire length of the pump laser, it emerges as a train of amplified pulses with shortened durations. Since *UH*-wave mediation has a smaller growth rate, it takes longer time, and equivalently, a longer pump laser and plasma length, to achieve the same compression of the seed pulse.

B. Limiting effects

Although the amplification rate is reduced for *UH* mediation, the growth rates of competing instabilities are reduced more. Therefore, one can use longer pumps than allowed in unmagnetized plasmas to amplify the seed pulse when the media become magnetized. For example, one of the most competitive instabilities is the modulational instability of the seed pulse, whose growth rate[27] $\gamma_M = \omega_3^2|a_2|^2/8\omega_1\gamma_3^2$ is reduced by an additional factor of $\gamma_3 > 1$. After a few exponentiations, the modulational instability causes the leading spike in the pulse train to break up, and thereof limits the allowable amplification time t_M. Allowing for the possibility that subdominant spikes in the pulse train may further grow,[53,54] we may estimate a lower bound[27] $t_M \propto \omega_3^{-1}\gamma_3^{4/3}$. Notice that the exponent of γ_3 is larger than one. In fact, this exponent is larger than 3/2 in particle-in-cell (PIC) simulations.[55] The net consequence of a smaller amplification rate but a longer allowable amplification time is thus a higher achievable pulse intensity when we magnetize the plasma medium.

In addition to suppressing competing instabilities, replacing plasma density with magnetic fields also reduces wave damping, which dissipates wave energy that could otherwise be used to amplify the laser pulse. Since collisional damping rates of *EM* waves are $\nu_{1,2} \simeq \nu_{ei}\omega_p^2/2\omega_{1,2}^2$, where $\nu_{ei} = n_e Z^2 e^4 \Lambda/(4\pi\epsilon_0)^2 m_e^2 v^3$ is the electron-ion collision frequency, the damping rates of *EM* waves scale with plasma density as $\nu_{1,2} \propto n_e^2$, as expected of two-body collisions. Therefore, when plasma density is replaced by magnetic fields, collisional damping of *EM* waves can be substantially reduced. In addition to collisional damping, the plasma wave also suffers from collisionless damping. Although linear collisionless damping exactly vanishes when the plasma wave propagates perpendicular to the magnetic field,[15] nonlinear mechanisms such as stochastic heating[56,57] and surfatron acceleration,[58,59] can still damp the plasma wave. Since collisionless damping is due to phase mixing, its rate scales as $\nu_3 \propto n_e$. Therefore, collisionless damping is also reduced when magnetized plasmas are used instead.

While moderate magnetic fields improve the performance of laser pulse compression, it is not favorable to impose a magnetic field that is too strong due to wakefield generation. Laser wakefield is generated when ponderomotive force of the laser expels electrons to form plasma bubbles. When plasma density is reduced, wakefield can thus be excited more easily. Moreover, as the magnetization factor increases, the spectrum of the wakefield broadens[60] and electromagnetic components of the wakefield enlarge.[55] Consequently, magnetized wakefield contains larger degrees of freedom, which allow the wakefield to partition a larger fraction of the total energy during nonlinear interactions. Energy in the wakefield can thereafter be transferred irreversibly to accelerate electrons. In addition to wakefield acceleration in the direction of laser propagation, electrons are also accelerated in the perpendicular direction due to the magnetic field, which allows electrons to enter and leave plasma bubbles in the transverse direction. Therefore, when magnetic fields increase beyond the optimal value, magnetized wakefield inhibits further growth of the laser pulse.

Fortunately, the vulnerability due to electromagnetic wakefield generation may be compensated by the resilience of magnetized plasmas to wavebreaking. Wavebreaking of the plasma wave is what limits the viable pump laser intensity in unmagnetized plasmas. When the pump intensity exceeds the wavebreaking threshold, the excited plasma wave becomes so strong that the quivering electrons outrun the wave, leading to a collapse of the plasma wave envelope. However, when the plasma density is replaced by a magnetic field, the plasma wave electric field is reduced, and the background magnetic field provides an additional restoring force. Therefore, the plasma wave is able to maintain its coherence even when the pump laser has exceeded the wavebreaking threshold.[55] Until a larger phase mixing threshold is reached, we can use more intense pump lasers than allowed in unmagnetized plasmas to amplify the seed pulse to higher intensity.

C. Validation using PIC simulations

The prediction that applying a moderate magnetic field improves the performance of laser pulse compression has been verified using particle-in-cell (PIC) simulations. In a set

of one-dimensional PIC simulations,[55] we use a 1.0-μm pump laser, with initial intensity $I_{10} = 3.5 \times 10^{14}\mathrm{W/cm^2}$, to compress a counter-propagating 1.1–μm seed pulse, whose initial intensity $I_{20} = 1.8 \times 10^{13}\mathrm{W/cm^2}$ and initial duration $\Delta t_{20} = 33$ fs. Given the pump and the seed lasers, we apply a magnetic field transverse to the direction of laser propagation, and reduce the plasma density accordingly to maintain the resonance conditions [Fig. 2(a)]. When there is no magnetic field (black line), pulse compression is mediated by Raman backscattering. After the initial exponential growth, the seed pulse enters the nonlinear compression stage, until its intensity saturates at $I_2 \approx 5.5 \times 10^{17}\mathrm{W/cm^2}$ due to the modulational instability. As we increase the magnetic field (color lines), the growth becomes slower, but the saturation is delayed. The net consequence is that the attainable final pulse intensity increases with the magnetic field, until an optimal field $B \approx 8.6$ MG is reached (red line), where the final pulse intensity is about twice of what is achievable using Raman compression. When a stronger magnetic field is applied (blue line), the seed pulse loses a substantial amount of energy to the wakefield, which inhibits further increase of the pulse intensity.

In addition to improving the performance in the optical regime, applying a magnetic field enables compression of short-wavelength pulses that cannot be compressed using unmagnetized plasmas. For example, a 10-nm soft x-ray laser is at the verge of what can be amplified using Raman compression.[22] At an even shorter wavelength, collisional damping becomes too strong. The total damping could have been alleviated by increasing the plasma temperature, if it were not due to collisionless damping, which increases with the plasma temperature. Therefore, the operation window in the plasma parameter space is almost closed.[27] In one-dimensional PIC simulations,[61] the 11-nm seed pulse, whose initial intensity $I_{20} = 1.4 \times 10^{18}\mathrm{W/cm^2}$ and initial duration $\Delta t_{20} = 1.5$ fs, barely grows when pumped by the $I_{10} = 1.4 \times 10^{18}\mathrm{W/cm^2}$ laser [Fig. 2(b), black]. However, by replacing plasma density with a 0.8 GG magnetic field, the effective growth rate becomes much larger (purple). This is because although the undamped growth rate $\gamma_0 \propto n_e^{1/2}$ is reduced in lower density plasmas, the collisionless damping $\nu_3 \propto n_e$ and the collisional damping $\nu_{1,2} \propto n_e^2$ are reduced more substantially. Therefore, faster effective growth is possible when we magnetize the plasma medium, using which compression of soft x-ray pulses beyond the reach of previous methods becomes possible.

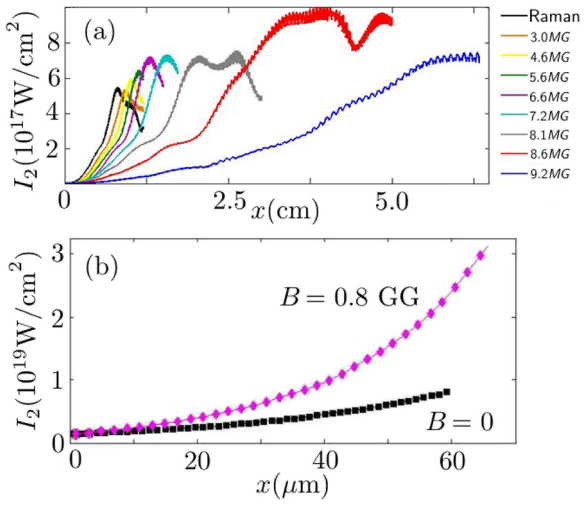

FIG. 2. Applying a transverse magnetic field improves the performance of plasma-based laser pulse compression, as shown here using 1D PIC simulations. For a 1-μm optical pulse (a), using a longer plasma and an optimal magnetic field (red line), the final pulse intensity is twice of what is achievable using unmagnetized Raman (black line). The initial pump intensity $I_{10} = 3.5 \times 10^{14}\mathrm{W/cm^2}$, and the 1.1-$\mu$m seed has initial intensity $I_{20} = 1.8 \times 10^{13}\mathrm{W/cm^2}$ and initial duration $\Delta t_{20} = 33$ fs. For a 10-nm x-ray pulse (b), replacing plasma density with a transverse magnetic field on giga-Gauss scale alleviates strong damping. Consequently, magnetized pulse compression becomes possible (purple), while unmagnetized amplification can barely work (black). The pump intensity $I_{10} = 1.4 \times 10^{18}\mathrm{W/cm^2}$, and the 11-nm seed pulse has $I_{20} = 1.4 \times 10^{18}\mathrm{W/cm^2}$ and $\Delta t_{20} = 1.5$ fs.

IV. LIGHT PROPAGATION IN RELATIVISTIC-QUANTUM REGIME

While mega-Gauss magnetic fields introduce new phenomena and applications in the classical regime, an even stronger giga-Gauss magnetic field may already enable us to probe relativistic-quantum physics.[28] To see when relativistic-quantum effects are important, we can compare energy scales in the system. The typical energy scales of plasmas are thermal energy k_{BT}, Fermi energy ϵ_F, plasmon energy $\epsilon_p = \omega_p\hbar$, and gyro energy $\epsilon_g = \Omega_e\hbar$. The energy scales of the fields are electric energy $\epsilon_E = \sqrt{eEc\hbar}$, magnetic energy $\epsilon_B = \sqrt{eBc^2\hbar}$, photon energy $\epsilon_\gamma = \omega_\gamma\hbar$, and ponderomotive energy U_p. Relativistic effects are important when any energy scale becomes comparable to the electron rest energy m_ec^2, and quantum effects are important whenever non-thermal energy ϵ_* dominates the thermal energy. An example where both relativistic and quantum effects are important is the magnetosphere of an x-ray pulsar. The typical magnetic field $B \sim 10^{12}$ G corresponds to $\epsilon_B \sim 100$ keV. Since ϵ_B is comparable to $m_ec^2 \approx 511$ keV, relativistic effects are important. At the same time, ϵ_B is much higher than the thermal energy $k_BT \sim 10$ keV, which makes quantum effects important. Although magnetic fields of such strength are not yet available in laboratory, it turns out that small relativistic-quantum corrections may already become observable in giga-Gauss magnetic field through Faraday rotation.

A. Dispersion relation in QED plasmas

To interpret signals from strongly magnetized plasmas, it is imperative that we understand how light propagates in the relativistic-quantum regime. Propagation of small amplitude waves, such as photons, is governed by the linear dispersion relation. The dispersion relation can be derived from the linearized momentum space wave equation, which can be written in a Lorentz-invariant and gauge-invariant form $(k^\mu k^\nu - k^2 g^{\mu\nu} + \hat{\Sigma}^{\mu\nu})A_\nu = 0$, where k^μ is the wave 4-momentum and $g^{\mu\nu}$ is the Minkowski metric. The response tensor $\hat{\Sigma}^{\mu\nu}$, which satisfies the Ward-Takahashi identity $\hat{\Sigma}^{\mu\nu}k_\nu = k_\mu\hat{\Sigma}^{\mu\nu} = 0$, describes reactions felt by photons, as they polarize both the plasma medium and the vacuum. Since the dispersion relation is gauge invariant, we can, for

example, choose the temporal gauge $A_0 = 0$. In this gauge, the linear dispersion relation becomes

$$\det\begin{pmatrix} \omega^2 - k_\parallel^2 + \hat{\Sigma}^{11} & \hat{\Sigma}^{12} & k_\perp k_\parallel + \hat{\Sigma}^{13} \\ \hat{\Sigma}^{21} & \omega^2 - \boldsymbol{k}^2 + \hat{\Sigma}^{22} & \hat{\Sigma}^{23} \\ k_\perp k_\parallel + \hat{\Sigma}^{31} & \hat{\Sigma}^{32} & \omega^2 - k_\perp^2 + \hat{\Sigma}^{33} \end{pmatrix} = 0. \tag{14}$$

Here, we have used the natural units $\hbar = c = \epsilon_0 = 1$, and chosen a coordinate system in which the wave 4-momentum $k^\mu = (\omega, k_\perp, 0, k_\parallel)$. In this form, it is easy to recognize that the response tensor $\hat{\Sigma}^{ij} = \omega^2 \chi^{ij}$ is related to the linear susceptibility.

While the dispersion relation is formally identical to that in the classical regime, relativistic-quantum physics is encoded in the response tensor. As an example, let us consider the response tensor of a magnetized scalar-QED plasma in its ground state, when charged-particle responses dominate the vacuum response. In the coordinate system where $\mathbf{B}_0 = (0, 0, B_0)$, the diagonal components of the response tensor are[28]

$$\begin{aligned} \hat{\Sigma}^{11} &= -\frac{m\omega_p^2}{2m_0} \sum_{\varsigma=\pm1} \kappa_\varsigma^2 \mathbb{K}_\varsigma^{(1)}, \\ \hat{\Sigma}^{22} &= \hat{\Sigma}^{11} - \frac{m\omega_p^2}{2m_0} \sum_{\varsigma=\pm1} \kappa_\perp^2 (\mathbb{K}_\varsigma^{(0)} - 2\mathbb{K}_\varsigma^{(1)}), \\ \hat{\Sigma}^{33} &= -\frac{m\omega_p^2}{m_0} \left(1 + \frac{1}{2} \sum_{\varsigma=\pm1} \kappa_\parallel^2 \mathbb{K}_\varsigma^{(0)}\right), \end{aligned} \tag{15}$$

where summation over charged species is implied. In the above formulas, $\omega_p^2 = e^2 n_0/m$ is the plasma frequency and $m_0 = \sqrt{m^2 + eB_0}$ is the shifted ground state mass. The summation over $\varsigma = \pm 1$ corresponds to the summation of the s-channel and the t-channel Feynman diagrams. Inside the summations, $\kappa^\mu = l_B k^\mu/2$ is the wave 4-momentum normalized by the magnetic de Broglie wavelength $l_B = \sqrt{2/eB_0}$. The kernel of the propagator $\kappa_\varsigma^2 = \kappa_0^2 - \kappa_\parallel^2 + \varsigma \varrho_0 \kappa_0$, where $\varrho^\mu = l_B(m_0, 0, 0, 0)$ is the normalized 4-momentum of particles in the ground state. For conciseness, we denote $\mathbb{K}_\varsigma^{(n)} := \mathbb{K}(\kappa_\varsigma^2 - n, \kappa_\perp^2)$, where the $\mathbb{K}$-function is related to the confluent hypergeometric function ${}_1F_1(a; b; z)$ by $\mathbb{K}(x, z) := {}_1F_1(1; 1 - x; -z)/x$. Similarly, the off-diagonal components of the response tensor can be expressed in terms of the $\mathbb{K}$-function as[28]

$$\begin{aligned} \hat{\Sigma}^{12} &= -\hat{\Sigma}^{21} = -i\frac{m\omega_p^2}{2m_0} \sum_{\varsigma=\pm1} \varsigma \kappa_\varsigma^2 (\mathbb{K}_\varsigma^{(1)} - \mathbb{K}_\varsigma^{(0)}), \\ \hat{\Sigma}^{23} &= -\hat{\Sigma}^{32} = +i\frac{m\omega_p^2}{2m_0} \sum_{\varsigma=\pm1} \varsigma \kappa_\perp \kappa_\parallel (\mathbb{K}_\varsigma^{(1)} - \mathbb{K}_\varsigma^{(0)}), \\ \hat{\Sigma}^{31} &= +\hat{\Sigma}^{13} = -\frac{m\omega_p^2}{2m_0} \sum_{\varsigma=\pm1} \kappa_\perp \kappa_\parallel \mathbb{K}_\varsigma^{(1)}. \end{aligned}$$

The confluent hypergeometric function arises when we compute the response tensor by summing over all transitions between relativistic Landau levels.

B. Modifications to Faraday rotation

As a special case, consider photon propagation parallel to the magnetic field, in which case relativistic-quantum effects modify Faraday rotation. For exact parallel propagation $k_\perp = 0$, the $\mathbb{K}$-functions take special values $\mathbb{K}_\varsigma^{(n)} = 1/(\kappa_\varsigma^2 - n)$. Substituting these special values into the dispersion relation, it is straightforward to show that the two *EM* eigenmodes are the *R* wave, which satisfies $n^2 = R$, and the *L* wave, which satisfies $n^2 = L$, where $n^2 = c^2 k_\parallel^2/\omega^2$ is the refractive index, and the permittivities[28]

$$R = 1 - \sum_s \frac{m_s \omega_{ps}^2}{m_{s0}\omega^2} \frac{\omega^2 - k_\parallel^2 - 2m_{s0}\omega}{\omega^2 - k_\parallel^2 - 2(m_{s0}\omega + m_s\Omega_s)}, \tag{16}$$

$$L = 1 - \sum_s \frac{m_s \omega_{ps}^2}{m_{s0}\omega^2} \frac{\omega^2 - k_\parallel^2 + 2m_{s0}\omega}{\omega^2 - k_\parallel^2 + 2(m_{s0}\omega - m_s\Omega_s)}. \tag{17}$$

In the classical limit $\omega, k_\parallel, \Omega \ll m$, the above formulas recover the classical results. In the opposite limit, relativistic-quantum effects may substantially modify the dispersion relations.

Since the *R* wave and the *L* wave of the same frequency have different phase velocities, when they combine to form a linearly polarized wave, the wave polarization vector rotates at a rate

$$\frac{d\psi}{d\zeta} = \pi \Delta n. \tag{18}$$

Here, ψ is the polarization angle, $\zeta = z/\lambda_0$ is the distance of propagation normalized by the vacuum wavelength $\lambda_0 = 2\pi c/\omega$, and $\Delta n = n_L - n_R$ is the difference in refractive indexes between the *L* wave and the *R* wave of the same frequency. In an electron-ion plasma, since $m_i \gg m_e$, the dominant contribution comes from electrons. Keeping only electron terms in the dispersion relations, the refractive indexes

$$\begin{aligned} n_{R/L}^2 = 1 &- \frac{m\Omega}{\omega^2} - \frac{m\omega_p^2}{2m_0\omega^2} \mp \frac{m_0}{\omega} \\ &\pm \sqrt{\left(\frac{m\Omega}{\omega^2} + \frac{m\omega_p^2}{2m_0\omega^2} \pm \frac{m_0}{\omega}\right)^2 \mp \frac{2m\omega_p^2}{\omega^3}}, \end{aligned} \tag{19}$$

where the upper signs correspond to the *R* wave and the lower signs correspond to the *L* wave. It is straightforward to check that in the classical limit $\omega, \omega_p, \Omega \ll m$, the above formulas recover the classical results. As a side remark, notice that in electron-positron plasmas with charge-conjugation symmetry, the Faraday rotation remains identically zero as in the classical case.

Although relativistic-quantum modifications remain small in giga-Gauss magnetic fields, they are boosted near the cutoff frequency of the *R* wave, where Faraday rotation is maximized. Suppose we measure Faraday rotation by passing multiple linearly polarized lasers of slightly different frequencies through the same plasma, then the relativistic-quantum formula predicts a different frequency dependence

than expected classically. To see the difference, one can subtract measured data from the classical prediction, and plot $\Delta\psi$ as a function of the laser frequency (Fig. 3). For example, in a gas jet plasma with density $n_e = 10^{19}\text{cm}^{-3}$, a magnetic field $B_0 = 10^8$ G results in a difference of $\sim 1^\circ/\lambda_0$ when the laser frequency approaches the R-wave cutoff $\sim$1.16 eV (red line). This discrepancy can be resolved if the measurement uncertainty is $\lesssim$1.5% at the classical cutoff, and $\lesssim$15 ppm at $\sim$0.1 eV above the cutoff. In a stronger magnetic field $B_0 = 10^9$ G, the difference is as large as $\sim 10^\circ/\lambda_0$ near the cutoff $\sim$11.5 eV (blue line). This discrepancy can be resolved if measurement uncertainty is $\lesssim$67% at the classical cutoff, and $\lesssim$0.13% at $\sim$0.1 eV above the cutoff. While corrections introduced by a 0.1 GG magnetic field are unlikely to be measurable, much larger corrections introduced by giga-Gauss magnetic fields might be discernible from noise and inhomogeneities.

V. SUMMARY AND DISCUSSION

In this paper, we review three research directions, addressing challenges and opportunities when strong magnetic fields become available. First, we provide a convenient formula for resonant three-wave coupling coefficient in magnetized plasmas [Eq. (6)]. Using this formula, we identify special angles where the scattering is polarization-, interference-, and energy-forbidden in a cold hydrogen plasma (Fig. 1). Away from these forbidden angles, coherent laser scattering in a magnetized plasma has a growth rate comparable to that of Raman backscattering. Consequently, magnetic fields may be applied to either suppress or enhance laser scattering at selected angles. Further analysis of thermal effects and wave damping in the presence of multiple laser beams may enable optimization of laser-plasma coupling in magnetized implosion experiments.

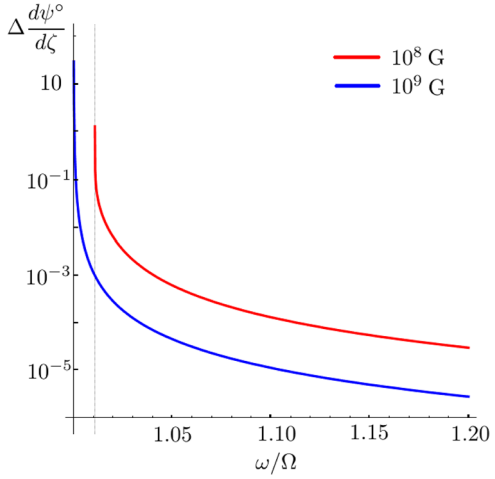

FIG. 3. Deviations of Faraday rotation from classical predictions can be used to measure relativistic-quantum corrections. In a gas jet plasma with density $n_e = 10^{19}\text{cm}^{-3}$, a 0.1 GG magnetic field (red) leads to a deviation $\Delta\psi$ of $\sim 1^\circ$ after the laser, whose frequency is near the R-wave cutoff, propagates by a vacuum wavelength λ_0. In a stronger 1 GG magnetic field (blue), a deviation as large as $\sim 10^\circ/\lambda_0$ may be observed using a laser whose frequency is slightly above the cutoff. Notice that the deviations fall precipitously when the laser frequency is above the classical cutoff. Therefore, for relativistic-quantum effects to be measurable, the laser frequency must be sufficiently close to the R-wave cutoff.

Second, we analyze benefits of applying magnetic fields in laser pulse compression. In addition to relaxing engineering constraints, substituting plasma density with a moderate magnetic field suppresses competing instabilities and reduces wave damping. These improvements enable us to use the magnetic field as an extra control variable to optimize the performance of 1-μm laser pulse compression [Fig. 2(a)]. Moreover, using upper-hybrid mediation, compression of soft x-ray pulses beyond the reach of unmagnetized schemes now becomes possible [Fig. 2(b)]. These results, obtained from simple analytical estimations and 1D PIC simulations, remain to be verified by more comprehensive simulations and ultimately by experiments. In addition to upper-hybrid mediation, the possibilities of using other magnetized plasma waves, such as Alfvén waves, hybrid waves, and Bernstein waves, to mediate pulse compression remain to be analyzed.

Finally, we speculate experimental possibilities of entering the relativistic-quantum regime using giga-Gauss magnetic fields, which are at the cusp of current feasibility. Although such magnetic fields are still much smaller than the Schwinger field, relativistic-quantum modifications may already become observable using Faraday rotation (Fig. 3), albeit very challenging. While results in cold scalar-QED plasmas may be instructive, laboratory plasmas are typically made of spinor particles at finite temperature. Therefore, spin and thermal effects on experimental observables remain to be studied. Beyond the perturbative regime, it might be possible to use a combination of a strong magnetic field and an intense laser to probe relativistic-quantum physics that cannot be probed by neither the magnetic field nor the laser alone. For this purpose, developing numerical schemes that can simulate relativistic-quantum plasmas will become indispensable.

ACKNOWLEDGMENTS

Special thanks to Dr. Qing Jia for carrying out PIC simulations on PPPL's Research Computing Center using the EPOCH code, and providing us with Fig. 2 in this paper. This research was supported by NNSA Grant No. DE-NA0002948, AFOSR Grant No. FA9550-15-1-0391, and DOE Grant No. DEAC02-09CH11466.

[1]I. Igumenshchev, A. Zylstra, C. Li, P. Nilson, V. Goncharov, and R. Petrasso, "Self-generated magnetic fields in direct-drive implosion experiments," Phys. Plasmas **21**, 062707 (2014).
[2]O. Gotchev, P. Chang, J. Knauer, D. Meyerhofer, O. Polomarov, J. Frenje, C. Li, M.-E. Manuel, R. Petrasso, J. Rygg *et al.*, "Laser-driven magnetic-flux compression in high-energy-density plasmas," Phys. Rev. Lett. **103**, 215004 (2009).
[3]J. Knauer, O. Gotchev, P. Chang, D. Meyerhofer, O. Polomarov, R. Betti, J. Frenje, C. Li, M.-E. Manuel, R. Petrasso *et al.*, "Compressing magnetic fields with high-energy lasers," Phys. Plasmas **17**, 056318 (2010).
[4]S. Fujioka, Z. Zhang, K. Ishihara, K. Shigemori, Y. Hironaka, T. Johzaki, A. Sunahara, N. Yamamoto, H. Nakashima, T. Watanabe *et al.*, "Kilotesla magnetic field due to a capacitor-coil target driven by high power laser," Sci. Rep. **3**, 1170 (2013).
[5]J. Santos, M. Bailly-Grandvaux, L. Giuffrida, P. Forestier-Colleoni, S. Fujioka, Z. Zhang, P. Korneev, R. Bouillaud, S. Dorard, D. Batani *et al.*, "Laser-driven platform for generation and characterization of strong quasi-static magnetic fields," New J. Phys. **17**, 083051 (2015).

[6]C. Goyon, B. Pollock, D. Turnbull, A. Hazi, L. Divol, W. Farmer, D. Haberberger, J. Javedani, A. Johnson, A. Kemp *et al.*, "Ultrafast probing of magnetic field growth inside a laser-driven solenoid," Phys. Rev. E **95**, 033208 (2017).
[7]M. Borghesi, A. MacKinnon, A. Bell, R. Gaillard, and O. Willi, "Megagauss magnetic field generation and plasma jet formation on solid targets irradiated by an ultraintense picosecond laser pulse," Phys. Rev. Lett. **81**, 112 (1998).
[8]M. Tatarakis, A. Gopal, I. Watts, F. Beg, A. Dangor, K. Krushelnick, U. Wagner, P. Norreys, E. Clark, M. Zepf *et al.*, "Measurements of ultrastrong magnetic fields during relativistic laser–plasma interactions," Phys. Plasmas **9**, 2244–2250 (2002).
[9]M. Tatarakis, I. Watts, F. Beg, E. Clark, A. Dangor, A. Gopal, M. Haines, P. Norreys, U. Wagner, M.-S. Wei *et al.*, "Laser technology: Measuring huge magnetic fields," Nature **415**, 280 (2002).
[10]U. Wagner, M. Tatarakis, A. Gopal, F. Beg, E. Clark, A. Dangor, R. Evans, M. Haines, S. Mangles, P. Norreys *et al.*, "Laboratory measurements of 0.7 GG magnetic fields generated during high-intensity laser interactions with dense plasmas," Phys. Rev. E **70**, 026401 (2004).
[11]M. J.-E. Manuel, C. K. Li, F. H. Séguin, J. Frenje, D. T. Casey, R. D. Petrasso, S. X. Hu, R. Betti, J. D. Hager, D. D. Meyerhofer, and V. A. Smalyuk, "First measurements of Rayleigh-Taylor-induced magnetic fields in laser-produced plasmas," Phys. Rev. Lett. **108**, 255006 (2012).
[12]L. Gao, P. Nilson, I. Igumenschev, S. Hu, J. Davies, C. Stoeckl, M. Haines, D. Froula, R. Betti, and D. Meyerhofer, "Magnetic field generation by the Rayleigh-Taylor instability in laser-driven planar plastic targets," Phys. Rev. Lett. **109**, 115001 (2012).
[13]L. Gao, P. Nilson, I. Igumenshchev, M. Haines, D. Froula, R. Betti, and D. Meyerhofer, "Precision mapping of laser-driven magnetic fields and their evolution in high-energy-density plasmas," Phys. Rev. Lett. **114**, 215003 (2015).
[14]J. Sheffield, D. Froula, S. H. Glenzer, and N. C. Luhmann, Jr., *Plasma Scattering of Electromagnetic Radiation: Theory and Measurement Techniques* (Academic Press, 2010).
[15]T. Stix, *Waves in Plasmas* (American Institute of Physics, 1992).
[16]J. F. Drake, P. K. Kaw, Y.-C. Lee, G. Schmid, C. S. Liu, and M. N. Rosenbluth, "Parametric instabilities of electromagnetic waves in plasmas," Phys. Fluids **17**, 778–785 (1974).
[17]Y. Shi, H. Qin, and N. J. Fisch, "Three-wave scattering in magnetized plasmas: From cold fluid to quantized Lagrangian," Phys. Rev. E **96**, 023204 (2017).
[18]W.-M. Wang, P. Gibbon, Z.-M. Sheng, and Y.-T. Li, "Magnetically assisted fast ignition," Phys. Rev. Lett. **114**, 015001 (2015).
[19]D. Barnak, J. Davies, R. Betti, M. Bonino, E. Campbell, V. Y. Glebov, D. Harding, J. Knauer, S. Regan, A. Sefkow *et al.*, "Laser-driven magnetized liner inertial fusion on omega," Phys. Plasmas **24**, 056310 (2017).
[20]R. Milroy, C. Capjack, and C. James, "Plasma laser pulse amplifier using induced Raman or Brillouin processes," Phys. Fluids **22**, 1922–1931 (1979).
[21]V. Malkin, G. Shvets, and N. Fisch, "Fast compression of laser beams to highly overcritical powers," Phys. Rev. Lett. **82**, 4448 (1999).
[22]V. Malkin, N. Fisch, and J. Wurtele, "Compression of powerful x-ray pulses to attosecond durations by stimulated Raman backscattering in plasmas," Phys. Rev. E **75**, 026404 (2007).
[23]A. Andreev, C. Riconda, V. Tikhonchuk, and S. Weber, "Short light pulse amplification and compression by stimulated Brillouin scattering in plasmas in the strong coupling regime," Phys. Plasmas **13**, 053110 (2006).
[24]M. R. Edwards, Q. Jia, J. M. Mikhailova, and N. J. Fisch, "Short-pulse amplification by strongly coupled stimulated Brillouin scattering," Phys. Plasmas **23**, 083122 (2016).
[25]M. R. Edwards, J. M. Mikhailova, and N. J. Fisch, "X-ray amplification by stimulated Brillouin scattering," Phys. Rev. E **96**, 023209 (2017).
[26]P. Maine, D. Strickland, P. Bado, M. Pessot, and G. Mourou, "Generation of ultrahigh peak power pulses by chirped pulse amplification," IEEE J. Quantum Electron. **24**, 398–403 (1988).
[27]Y. Shi, H. Qin, and N. J. Fisch, "Laser-pulse compression using magnetized plasmas," Phys. Rev. E **95**, 023211 (2017).
[28]Y. Shi, N. J. Fisch, and H. Qin, "Effective-action approach to wave propagation in scalar QED plasmas," Phys. Rev. A **94**, 012124 (2016).
[29]D. J. Kaup, A. Reiman, and A. Bers, "Space-time evolution of nonlinear three-wave interactions. I. Interaction in a homogeneous medium," Rev. Mod. Phys. **51**, 275–309 (1979).
[30]A. Sjölund and L. Stenflo, "Non-linear coupling in a magnetized plasma," Z. Phys. A: Hadrons Nucl. **204**, 211–214 (1967).
[31]J. J. Galloway and H. Kim, "Lagrangian approach to non-linear wave interactions in a warm plasma," J. Plasma Phys. **6**, 53–72 (1971).
[32]T. J. M. Boyd and J. G. Turner, "Three and four wave interactions in plasmas," J. Math. Phys. **19**, 1403–1413 (1978).
[33]B. K. Shivamoggi, "Kinetic theory of three-wave interaction in a magnetised, inhomogeneous plasma," Phys. Scr. **25**, 637 (1982).
[34]S. Ram, "Nonlinear scattering from electron Bernstein modes in a plasma," Plasma Phys. **24**, 885 (1982).
[35]T. J. M. Boyd and R. Rankin, "Kinetic theory of stimulated Raman scattering from a magnetized plasma," J. Plasma Phys. **33**, 303–319 (1985).
[36]B. I. Cohen, "Compact dispersion relations for parametric instabilities of electromagnetic waves in magnetized plasmas," Phys. Fluids **30**, 2676–2680 (1987).
[37]V. Stefan, N. Krall, and J. McBride, "The nonlinear eikonal relation of a weakly inhomogeneous magnetized plasma upon the action of arbitrarily polarized finite wavelength electromagnetic waves," Phys. Fluids **30**, 3703–3712 (1987).
[38]N. M. Laham, A. S. A. Nasser, and A. M. Khateeb, "Effects of axial magnetic fields on backward Raman scattering in inhomogeneous plasmas," Phys. Scr. **57**, 253 (1998).
[39]H. Sanuki and G. Schmidt, "Parametric instabilities in magnetized plasma," J. Phys. Soc. Jpn. **42**, 664–669 (1977).
[40]C. Grebogi and C. S. Liu, "Brillouin and Raman scattering of an extraordinary mode in a magnetized plasma," Phys. Fluids **23**, 1330–1335 (1980).
[41]I. Dodin and A. Arefiev, "Parametric decay of plasma waves near the upper-hybrid resonance," Phys. Plasmas **24**, 032119 (2017).
[42]B. C. Stuart, M. D. Feit, A. M. Rubenchik, B. W. Shore, and M. D. Perry, "Laser-induced damage in dielectrics with nanosecond to subpicosecond pulses," Phys. Rev. Lett. **74**, 2248–2251 (1995).
[43]F. Canova, O. Uteza, J.-P. Chambaret, M. Flury, S. Tonchev, R. Fechner, and O. Parriaux, "High-efficiency, broad band, high-damage threshold high-index gratings for femtosecond pulse compression," Opt. Express **15**, 15324–15334 (2007).
[44]S. Obenschain, S. Bodner, D. Colombant, K. Gerber, R. Lehmberg, E. McLean, A. Mostovych, M. Pronko, C. Pawley, A. Schmitt *et al.*, "The Nike KrF laser facility: Performance and initial target experiments," Phys. Plasmas **3**, 2098–2107 (1996).
[45]P. Emma, R. Akre, J. Arthur, R. Bionta, C. Bostedt, J. Bozek, A. Brachmann, P. Bucksbaum, R. Coffee, F.-J. Decker *et al.*, "First lasing and operation of an ångstrom-wavelength free-electron laser," Nat. Photonics **4**, 641–647 (2010).
[46]T. Ishikawa, H. Aoyagi, T. Asaka, Y. Asano, N. Azumi, T. Bizen, H. Ego, K. Fukami, T. Fukui, Y. Furukawa *et al.*, "A compact x-ray free-electron laser emitting in the sub-angstrom region," Nat. Photonics **6**, 540–544 (2012).
[47]S. Glenzer, B. MacGowan, N. Meezan, P. Adams, J. Alfonso, E. Alger, Z. Alherz, L. Alvarez, S. Alvarez, P. Amick *et al.*, "Demonstration of ignition radiation temperatures in indirect-drive inertial confinement fusion hohlraums," Phys. Rev. Lett. **106**, 085004 (2011).
[48]R. Craxton, K. Anderson, T. Boehly, V. Goncharov, D. Harding, J. Knauer, R. McCrory, P. McKenty, D. Meyerhofer, J. Myatt *et al.*, "Direct-drive inertial confinement fusion: A review," Phys. Plasmas **22**, 110501 (2015).
[49]R. Neutze, R. Wouts, D. van der Spoel, E. Weckert, and J. Hajdu, "Potential for biomolecular imaging with femtosecond x-ray pulses," Nature **406**, 752–757 (2000).
[50]H. N. Chapman, P. Fromme, A. Barty, T. A. White, R. A. Kirian, A. Aquila, M. S. Hunter, J. Schulz, D. P. DePonte, U. Weierstall *et al.*, "Femtosecond x-ray protein nanocrystallography," Nature **470**, 73–77 (2011).
[51]S. Weber, C. Riconda, L. Lancia, J.-R. Marques, G. Mourou, and J. Fuchs, "Amplification of ultrashort laser pulses by Brillouin backscattering in plasmas," Phys. Rev. Lett. **111**, 055004 (2013).
[52]M. J. Hay, E. J. Valeo, and N. J. Fisch, "Geometrical optics of dense aerosols: Forming dense plasma slabs," Phys. Rev. Lett. **111**, 188301 (2013).
[53]V. Malkin, Z. Toroker, and N. Fisch, "Exceeding the leading spike intensity and fluence limits in backward Raman amplifiers," Phys. Rev. E **90**, 063110 (2014).
[54]I. Barth, Z. Toroker, A. A. Balakin, and N. J. Fisch, "Beyond nonlinear saturation of backward Raman amplifiers," Phys. Rev. E **93**, 063210 (2016).
[55]Q. Jia, Y. Shi, H. Qin, and N. J. Fisch, "Kinetic simulations of laser parametric amplification in magnetized plasmas," Phys. Plasmas **24**, 093103 (2017).

[56]C. F. Karney, "Stochastic ion heating by a lower hybrid wave," Phys. Fluids **21**, 1584–1599 (1978).
[57]C. F. Karney, "Stochastic ion heating by a lower hybrid wave: II," Phys. Fluids **22**, 2188–2209 (1979).
[58]R. Sagdeev and V. Shapiro, "Influence of transverse magnetic field on Landau damping," JETP Lett. **17**, 279–282 (1973), see https://www.osti.gov/biblio/4445084.
[59]J. M. Dawson, V. K. Decyk, R. W. Huff, I. Jechart, T. Katsouleas, J. N. Leboeuf, B. Lembege, R. M. Martinez, Y. Ohsawa, and S. T. Ratliff, "Damping of large-amplitude plasma waves propagating perpendicular to the magnetic field," Phys. Rev. Lett. **50**, 1455–1458 (1983).
[60]A. Holkundkar, G. Brodin, and M. Marklund, "Wakefield generation in magnetized plasmas," Phys. Rev. E **84**, 036409 (2011).
[61]Q. Jia, private communication (2016).